



# A new hyper-viscoelastic model for investigating rate dependent mechanical behavior of dual cross link self-healing hydrogel

A. Ghorbanoghli, K. Narooei\*

Department of Materials Science and Engineering, K. N. Toosi University of Technology, Tehran, Iran



## ARTICLE INFO

### Keywords:

Hyper-viscoelastic  
Self-healing  
Hydrogel  
Relaxation  
Preconditioning

## ABSTRACT

Self-healing hydrogels have been considered as an appropriate material for the biomechanical applications. Time-dependency and hyperelasticity are the significant mechanical behavior of these materials. In this research, a new hyperelastic strain energy function based on the polynomial-logarithmic terms was generalized to hyper-viscoelastic model for investigating the mechanical behavior of the dual cross self-healing hydrogel. The model parameters were determined by fitting with the experimental results of Long et al. and the material stability of the model in the pure shear and balance biaxial modes were investigated. It was observed the minimum strain rate for considering the rate dependent behavior is 0.003/s and below of this threshold the rate-dependent behavior could be neglected. The relaxation behavior of the hydrogel was simulated and results represented a good agreement with the experimental results. By ensuring the material stability, the cyclic loading was simulated and it was observed after three cycles the preconditioned state could be reached. Moreover, it was observed the energy dissipation depends on the loading-unloading rates. The hyper-viscoelastic model was used to simulate the healing process in the ABAQUS software using the VUMAT user subroutine. It was seen at least 300 s should be considered between the load/unload cycles to observe the healing phenomenon.

## 1. Introduction

Hydrogels are three-dimensional networks composed of hydrophilic polymer chains, which possess the ability to absorb a large amount of water up to thousands of their dry weight. Hydrogels are widely recognized as important biomaterials in biomedical and pharmaceutical industries such as wound healing, delivery carriers for drugs and genes [1]. Moreover, they used in the biomechanical applications as the replacement materials for body tissues and support for tissue growth [2]. Hydrogels also could be used as smart biomaterials and are ideal candidates for self-folding purpose due to their unique features like sensitivity to diverse stimuli, considerable shape and volume variation, excellent biocompatibility and bio-degradability [3]. Having not suitable mechanical properties, simple hydrogels cannot be appropriately used for mimicking natural tissues. Therefore, different methods have been developed to modify the mechanical properties of hydrogels such as adding nanoparticles [4,5] and using hydrogels with dual network structures [6,7]. Dual cross self-healing hydrogels are consist of a stiff network (with temporary physical bonds) and a soft network which is lightly cross-linked and extensible [8]. Under different type of stresses, the physical bonds break and they could reattach and form the network again after the deformation (healing). From the experimental results, it was understood that the mechanical behavior of these materials is not

only hyperelastic but also time dependent. Thereby, finding a proper hyper-viscoelastic constitutive model to characterize the mechanical behavior of these materials is very demanding.

According to the hyperelastic properties of the hydrogels and soft tissues, many efforts have been done to develop hyperelastic constitutive equations for modeling the mechanical behavior of these materials. Most of the hyperelastic models have been based on a strain energy function [9] as the logarithmic, exponential, power, and polynomial functions of principal stretches or invariants of the Cauchy-Green deformation tensor [10]. Hosseinzadeh et al. employed some hyperelastic strain energy functions to investigate the mechanical behavior of the demineralized and deproteinized bovine cortical femur bones [11]. They showed the exponential based hyperelastic strain energy represents a better agreement to the experimental data in comparison to the Ogden and Mooney-Rivlin models. Elyasi et al. used the general exponential model for predicting the mechanical behavior of extensor apparatus. By using this model they performed finite elements (FE) simulation of extensor flexion in the distal interphalangeal (DIP) joint [12]. Sasson et al. studied the hyperelastic behavior of chitosan hydrogels for nucleus pulposus replacement [13]. They performed the confined compression test on a sample and obtained the material parameters of different hyperelastic models to find the best model in FE simulations. Hamzehei et al. employed 3D printing technique to fabricate structures from TPU and

\* Corresponding author.

E-mail address: [knarooei@kntu.ac.ir](mailto:knarooei@kntu.ac.ir) (K. Narooei).

simulations based on the Marlow hyperelastic model showed the ability of the model to predict the behavior of the structures [14]. Zhao et al. conducted numerical simulations based on the Mooney-Rivlin hyperelastic theory to understand the internal stress distribution and possible failure of a nanofiber-reinforced hydrogel under the compression to investigate the possibility of using this hydrogel as a suitable scaffold in tissue engineering [15]. According to the literature review on the hyperelastic models, it could be concluded that the suitable model cannot be selected priori due to the nonlinear response of materials.

Since experimental tests showed the viscoelastic behavior of hydrogels, some researchers have taken into account the time-dependent behavior of materials in their studies. Creep [16–18], relaxation [19–21], and strain rates dependence of stress-strain curves in monotonic loadings (ramp test) [6,22–24] are three phenomena which proof the time-dependent behavior of Hydrogels. In order to mathematically describe the hyper-viscoelasticity, some studies have been done using Maxwell model [22,25]. On the other hand, some researchers used the Prony series to make the hyperelastic models suitable for time-dependent characterization. Ravikumar et al. found that using the Ogden model with a single term of Prony series is adequate to capture the response of a ballistic gelatin in surgical strain rates [26]. Narooei and Arman used an exponential based hyperelastic model with two terms of the Prony series to describe the mechanical behavior of the TPE gel tissue and they used the approach of Goh et al. to determine the material parameters of the model [27,28]. They also performed a finite element simulation of the Kolsky bar test to show the response of the TPE gel in high strain rates.

Soft materials usually are subjected to loading and unloading stresses like in energy absorbents and body organs. Therefore, many cyclic loading tests are performed to investigate the mechanical behavior of the soft materials. The Mullins effect, softening, energy dissipation, preconditioning, and self-recovery are the most significant phenomena which can be observed in the study of cyclic loadings [8,29–31]. The viscosity and Mullin effects are the two common sources for energy dissipation in the cycle loadings. Dorfmann and Ogden presented a constitutive model considering the Mullin effect in the reinforced rubbers that could separately capture the stress softening and residual strain effects [31]. Lu et al. used a rheological model to investigate the mechanical behavior of soft materials incorporating viscoelasticity and Mullin effect [32]. The other important matter due to viscoelasticity of materials is preconditioning. The preconditioning is a significant concept for investigation of the mechanical behavior of the soft tissues, since their actual mechanical properties could be determined after the preconditioning. Gefen and Margulies showed that the shear modulus of the conditioned brain is different from the preconditioned one [33]. Also, in clinical applications the preconditioning is a very significant phenomenon which should be considered [34]. For example, Kousa et al. showed the importance of grafts preconditioning in anterior cruciate ligament (ACL) reconstruction to reduce the residual displacements [35]. Hydrogels, like other soft materials, usually are preconditioned before mechanical tests. Johnson et al. expressed that their experimental errors would have been favorably reduced if they had preconditioned the hydrogel specimens [36]. Marra et al. used three and Millon et al. used ten cycles with different strains to reach preconditioned state for mechanical characterization of poly vinyl alcohol hydrogel [37,38].

According to the above literature review on the soft materials characterization, it can be found that an accurate model, which could take into account nonlinear elasticity and time dependency, would be a great desire for investigating the mechanical behavior of dual cross self-healing hydrogels. For this purpose, in this paper, we proposed a phenomenological model consisting of the polynomial-logarithmic hyperelastic part and the Prony series for considering the viscoelastic behavior. It was observed that the model could fit the experimental results of the dual cross self-healing hydrogel [8]. By using the proposed model, the number of cycles for preconditioning, healing time, and the mechanical behavior in different strain rates were predicted.

## 2. Hyper-viscoelastic model

The hyper-viscoelastic model consists of two parts, deformation dependent function with the dimensions of stress ( $S_0(C)$ ) and a dimensionless time-dependent function ( $g(t)$ ) as follows [27,39]:

$$S(C, t) = S_0(C)g(t) \quad (1)$$

where  $S$  is the second Piola-Kirchhoff stress tensor due to deformation,  $t$  is time, and  $C$  is the right Cauchy-Green deformation tensor. The strain-dependent part could be defined with a linear elasticity or hyperelasticity and the time-dependent part is represented by the Prony series as [27,28]:

$$g(t) = g_\infty + \sum_{i=1}^N g_i e^{-\frac{t}{\tau_i}} \quad (2)$$

here  $N$  is the number of series terms,  $\tau_i$  is the relaxation time,  $g_\infty$  and  $g_i$  are the dimensionless constants with the following properties [27]:

$$\begin{aligned} 0 < g_\infty &\leq 1 \\ 0 &\leq g_i < 1 \\ g_\infty + \sum_{i=1}^N g_i &= 1 \end{aligned} \quad (3)$$

**Eq. (1)** only can be used in the case of creep or relaxation tests (step loading) and when the ramp loading is being studied, the time-dependent stress is calculated using the convolution integral as [40]:

$$S(C, t) = \int_{-\infty}^t g(t-v) \frac{dS_0(C)}{dv} dv \quad (4)$$

In order to define the deformation dependent function in **Eq. (1)** (or **Eq. (4)**), a hyperelastic strain energy function should be used. Polynomial and Ogden hyperelastic functions are the most famous models which are used in the field of nonlinear elasticity [41,42]. In this research, a polynomial-logarithmic model was used as the hyperelastic strain energy to obtain accurate results:

$$W(C) = A_1(I_1 - 3) + A_2(I_2 - 3) + A_3(\ln \frac{I_1}{3}) + A_4(\ln \frac{I_2}{3}) + \frac{1}{K}(I_3 - 1) \quad (5)$$

where  $W$  is the hyperelastic strain energy function,  $A_i$ 's are the material parameters, and  $I_i$ 's are invariants of the right Cauchy-Green deformation tensor. Here  $K$  is a small number to impose the incompressibility condition. Using the strain energy function, the instantaneous second Piola-Kirchhoff stress tensor ( $S_0$ ) can be obtained as [43]:

$$S_0 = 2 \frac{\partial W}{\partial C} \quad (6)$$

By substituting of **Eq. (5)** in **Eq. (6)** and remembering the derivatives of the invariants with respect to tensor [43], the instantaneous second Piola-Kirchhoff stress tensor could be determined as:

$$\begin{aligned} S_0(C) &= 2 \frac{\partial W}{\partial C} = 2 \left( \frac{\partial W}{\partial I_1} \frac{\partial I_1}{\partial C} + \frac{\partial W}{\partial I_2} \frac{\partial I_2}{\partial C} + \frac{\partial W}{\partial I_3} \frac{\partial I_3}{\partial C} \right) \\ &= 2 \left( A_1 I + A_2(I_1 I - C) + \frac{A_3}{I_1} I + \frac{A_4}{I_2}(I_1 I - C) + \frac{1}{K} I_3 C^{-1} \right) \end{aligned} \quad (7)$$

here  $I$  is the second order identity tensor. Taking into account **Eq. (7)**, the strain-dependent (instantaneous) part of the hyper-viscoelastic model is determined. Substitution of **Eq. (2)** in **Eq. (4)**, the time-dependent part of the model also could be considered as [27]:

$$S(C, t) = g_\infty S_0(C) + \sum_{i=1}^N \int_{-\infty}^t g_i e^{-\frac{t-v}{\tau_i}} \frac{dS_0(C)}{dv} dv = g_\infty S_0(C) + \sum_{i=1}^N h_i(t) \quad (8)$$

where  $h_i$  is an abbreviation for the above integral and usually is called the heredity integral of viscous effect. Goh et al. estimated the heredity integral using the approximation proposed by Taylor et al. as [27,28]:

$$h_i(t_{n+1}) = e^{-\frac{\Delta t_{n+1}}{\tau_i}} h_i(t_n) + g_i \frac{1 - e^{-\frac{\Delta t_{n+1}}{\tau_i}}}{\frac{\Delta t_{n+1}}{\tau_i}} [S_0(C_{n+1}) - S_0(C_n)] \quad (9)$$

here the subscripts “ $n$ ” and “ $n+1$ ” show the variables at time “ $n$ ” and “ $n+1$ ” respectively;  $\Delta t_{n+1}$  characterizes the time increment between  $t_n$  and  $t_{n+1}$ . Substituting of Eq. (9) in Eq. (8), the time dependent stress at the current time could be determined from the stress in the previous time as [27]:

$$S(C_{n+1}, t_{n+1}) = g_\infty S_0(C_{n+1}) + \sum_{i=1}^N \left\{ e^{-\frac{\Delta t_{n+1}}{\tau_i}} h_i(t_n) + g_i \frac{1 - e^{-\frac{\Delta t_{n+1}}{\tau_i}}}{\frac{\Delta t_{n+1}}{\tau_i}} [S_0(C_{n+1}) - S_0(C_n)] \right\} \quad (10)$$

In Eq. (10),  $S(C_{n+1}, t_{n+1})$  is the stress at the current time (long term response) that could be calculated using the stress from the previous time  $S(C_n, t_n)$ . It is worth mentioning that  $S_0(C_{n+1})$  and  $S_0(C_n)$  are the instantaneous response of the stress tensor and it can be computed from Eq. (7). The significant consequence of this method is the simplicity of the derived equations in the programming for the computer-based simulations.

### 3. Determination of material parameters

As it could be seen from Eq. (5) there are 4 material parameters in the proposed hyperelastic model ( $A_1$  to  $A_4$ ). By choosing 3 terms of the Prony series ( $N=3$ ), seven more parameters ( $g_\infty, g_1, g_2, g_3$ , and  $\tau_1, \tau_2, \tau_3$ ) are appeared which means 11 unknown parameters should be determined. Different approaches are used to calculate the material parameters in different models but the main idea is minimizing the error between the experimental data and model using the least square method [26,44] or root mean square error (RMSE) [45]. Recently some researchers have used the finite element method to identify the material parameters of the constitutive model [18,46]. By using the initial guess and aiding of the finite element simulation, Fahimi et al. defined an objective function as the difference between the results of the finite element analysis and experiments [47]. Here, the same approach as Narooei and Arman was used to obtain the material parameters with the following error definition [27]:

$$\text{Error} = \frac{\|S - S_{Exp}\|_2}{\|S_{Exp}\|_2} \quad (11)$$

where “ $S$ ” is defined by Eq. (10) considering the uniaxial loading kinematic, “ $S_{Exp}$ ” could be extracted from the mechanical tests, and the symbol  $\|\cdot\|_2$  shows the  $L_2$  norm. The error defined here is referred as “SRSS” which is an acronym for the square root of the sum of squares. Using the function “fmincon” in MATLAB software and minimizing the error of Eq. (11), the material parameters of the constitutive equation could be calculated. The “fmincon” algorithm finds the minimum of a multivariable function under a specified constraint. There are different options in this algorithm that can be used to determine the upper bound, lower bound, and the constraint on the minimized function (here error function defined in Eq. (11)). Eq. (3) was used to define the upper bound, lower bound, and the relation between four variables ( $g_1, g_2, g_3, g_\infty$ ) as the constraint of minimization.

To find the material parameters, some researchers have used two different tests; tension test in order to define the hyperelastic parameters and relaxation for the time dependent part of the model [8]. However, here only by fitting the tension test in different strain rates of monotonic loading, the material parameters were determined; then the relaxation and cyclic loading tests were predicted to be clear the robustness of the model and fitting procedure.

### 4. Simulations

As mentioned in Section 3, using time discretization of Eq. (10) it is possible to implement the current hyper-viscoelastic model for the finite element simulation. To this goal, the VUMAT user subroutine of the

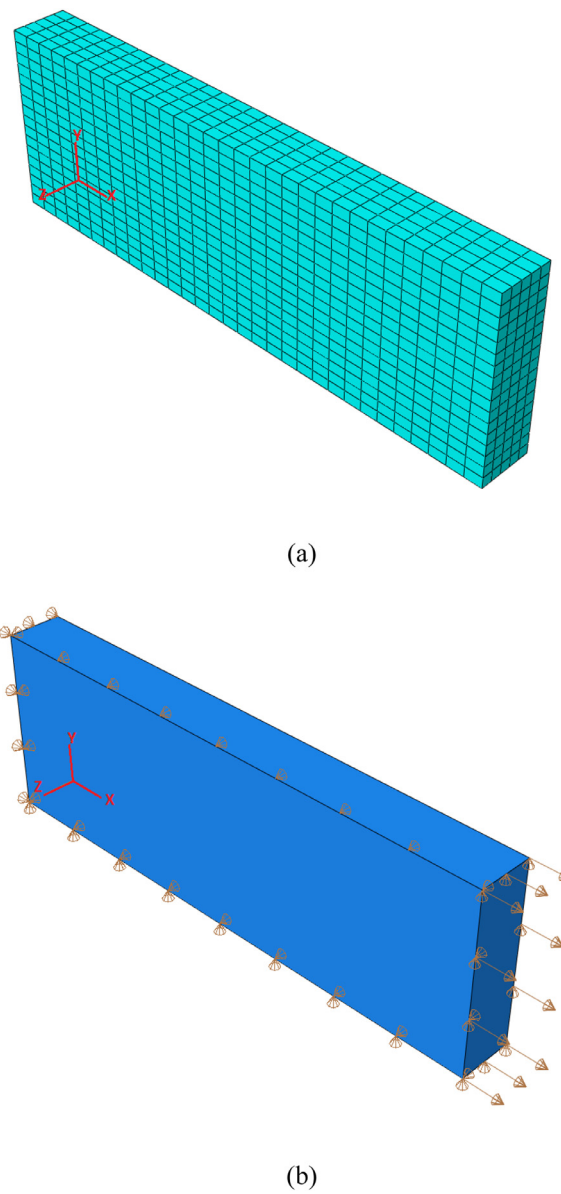


**Fig. 1.** Simulated geometry: (a) meshed sample (b) boundary conditions.

ABAQUS software was used. Although many different states of loading could be simulated, but investigation of the healing time could be the most appealing case to study. Self-healing behavior of the hydrogels is due to the chemical cross-links of the hydrogel network. However, neglecting the microstructure of the hydrogel and by using the proposed phenomenological hyper-viscoelastic model, the healing time of the hydrogel could be estimated. Healing time here is defined as the time between two loading-unloading cycles that sample completely recover its initial undeformed state. Considering the geometrical symmetry of test specimen, the simulated sample was assumed as  $2.5 \times 7.5 \times 0.75$  mm to take into account the similar geometry with the experimental samples of Long et al. [8]. The eight nodes linear brick element with reduced integration and hourglass control (C3D8R) were used to mesh the sample with 1745 elements and then deformed under five consecutive steps. At the first step, the sample was stretched to 15 mm with the strain rate of 0.03/s (loading) and then it was unloaded with the same strain rate (unloading). In the third step, the sample was kept for the desired time to consider the healing process. Finally, the second load-unload cycle was simulated like the steps one and two.

The geometry and applied boundary conditions can be seen in Fig. 1. Here 1/8 of real sample is considered instead of the real dimension (each

**Table 1**

Material parameters and relative error of proposed model for dual-cross self-healing hydrogel.

Hyperelastic	$A_1$ (Pa) $9.9274 \times 10^3$	$A_2$ (Pa) $9.8897 \times 10^{-5}$	$A_3$ (Pa) $3.3234 \times 10^{-4}$	$A_4$ (Pa) $2.2034 \times 10^{-4}$
Prony series	$g_\infty$ $1.5603 \times 10^{-1}$	$g_1$ $2.4857 \times 10^{-1}$	$g_2$ $4.6286 \times 10^{-1}$	$g_3$ $1.3254 \times 10^{-1}$
Relaxation	$\tau_1$ (s) 4.8125	$\tau_2$ (s) 1.0863	$\tau_3$ (s) $4.2177 \times 10^1$	
Relative error	$1.5642 \times 10^{-2}$			

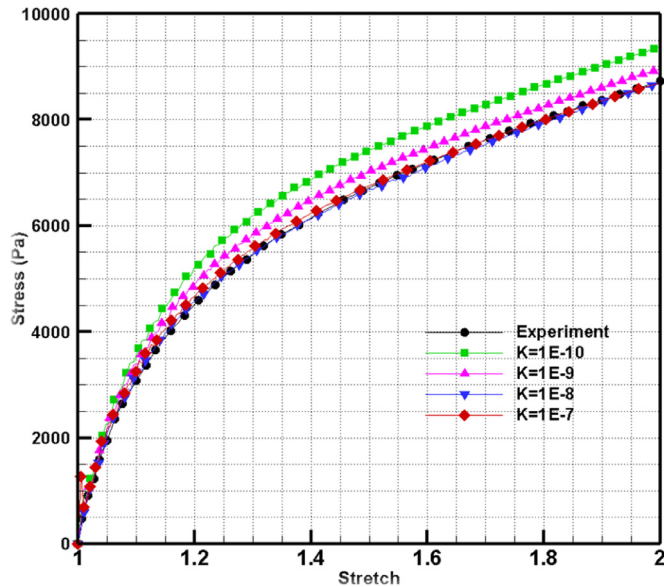


Fig. 2. Tension test simulation at different incompressibility parameter ( $K$ ) in strain rate of 0.03/s (experimental data [8]).

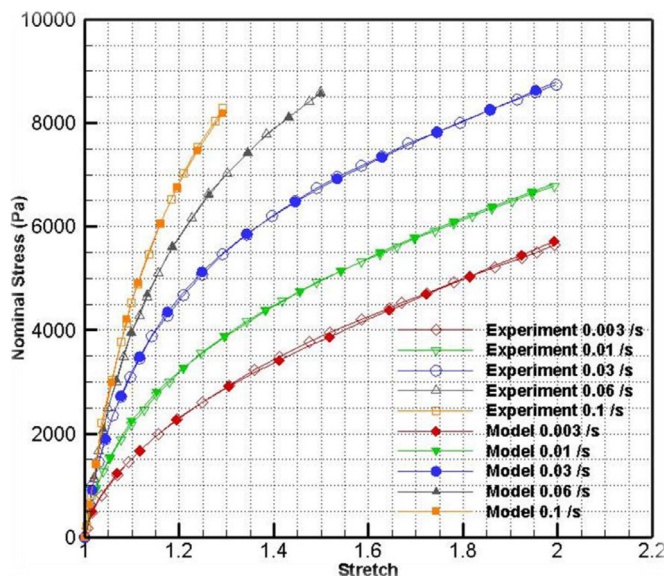


Fig. 3. Model prediction and experimental uniaxial tension data [8] in different strain rates.

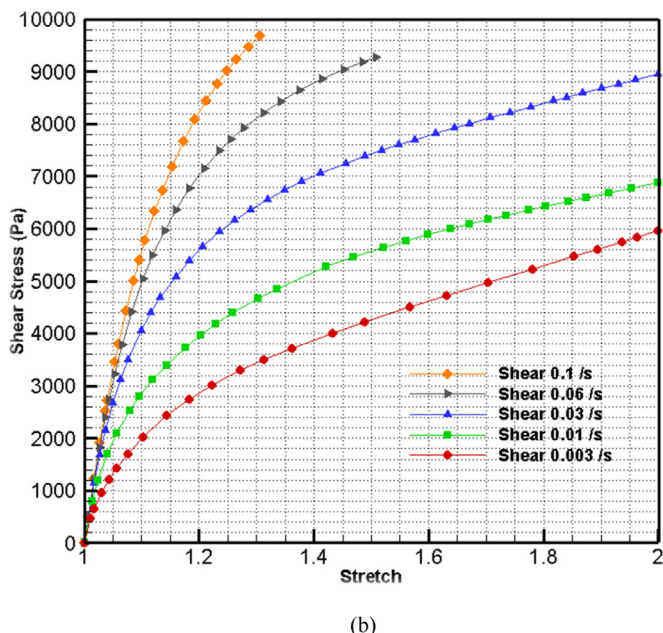
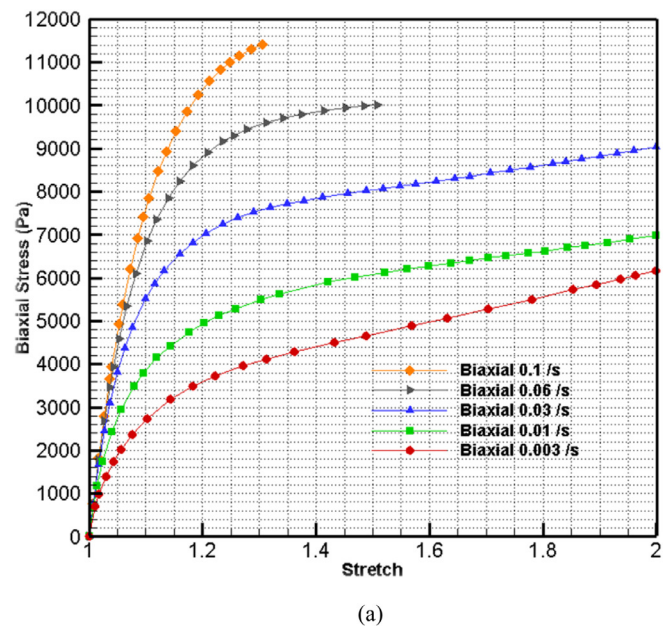
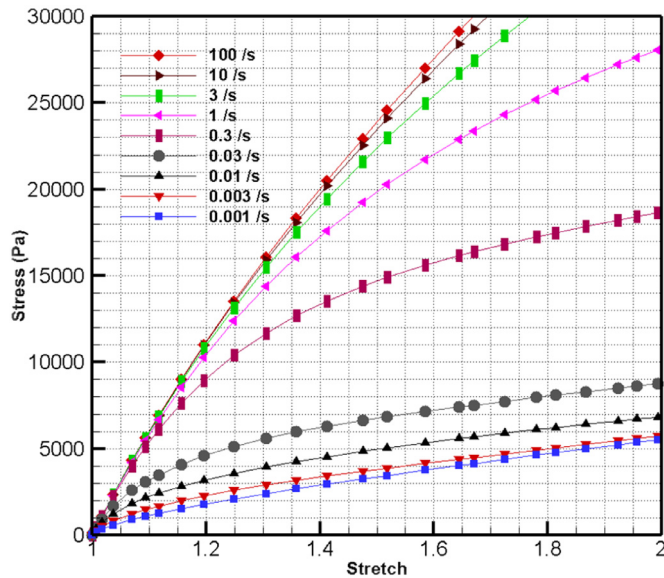


Fig. 4. Prediction of the proposed model in: (a) Balance biaxial and (b) pure shear modes.

length in the considered part is equal to the half of the real sample) to reduce the calculating time in ABAQUS. The YZ plane in Fig. 1(b) is constrained in X direction, the XZ plane is constrained in Y direction and the XY plane is constrained in Z direction in order to keep the geometrical symmetry. The appropriate velocity boundary condition was imposed to the right plane of sample to preserve the loading and unloading strain rates of the test protocol (as mentioned above). In the healing step, the velocity boundary condition of the right plane was removed to consider the healing under no constraint.

To obtain the optimum value of the incompressibility parameter ( $K$ ), the tension test with different values was performed in strain rate of 0.03/s as it is shown in Fig. 2. As it could be seen from Fig. 2, the value of  $10^{-8}$  could be considered as the optimum value of this parameter as by further decreasing of the incompressibility parameter no significant change in the results occurred.



**Fig. 5.** Model prediction of uniaxial tension at different strain rates.

## 5. Results and discussion

In order to demonstrate the ability of the current model for characterizing the time-dependent behavior of the dual-cross self-healing hydrogel, firstly the uniaxial tension test at different strain rates was investigated. Then by using the proposed model, the relaxation test results will be compared with the experimental data to show the model ability in different time-dependent conditions. Being confident, from the model results, the number of cycles for the desirable preconditioning and the healing time of the hydrogel will be estimated.

### 5.1. Relaxation test prediction

Long et al. carried out the uniaxial tensile, relaxation, and cyclic loading tests to investigate the time-dependent behavior of the dual cross-link self-healing hydrogel [8]. Here, we used the results of tension test at different strain rates of 0.003/s to 0.1/s to obtain the hyper-viscoelastic parameters. Multiple sets of the material parameters could be obtained in the fitting procedure and it was advised to choose the most appeared set [27,48]. Nevertheless, in the current research by imposing of the positive material parameters as a constraint in the minimization procedure of Eq. (11) a unique set of material parameters was obtained. The determined material parameters could be seen in Table 1.

Considering the material parameters of Table 1, the stress-stretch curves at different strain rates were calculated and the results could be seen in Fig. 3. As it could be seen in addition to the good agreement with experimental data, by increasing of strain rate the stress is increased in a constant stretch. The area under the stress-stretch curve before rupture could be considered as the ductility which here by investigating of Fig. 3, the optimum ductility could be achieved at strain rates 0.03/s.

To show the material stability, the prediction of the material behavior in the balanced biaxial and pure shear states using the proposed model was shown in Fig. 4. As it could be seen the model presents material stability in these modes and therefore it could be used in the finite element simulations. Long et al. used the Neo-Hookean hyperelastic function for the instantaneous response of the dual cross link hydrogel [8]. As in this model the second invariant of the Cauchy-Green deformation tensor is not appeared, it is prone to fail in the pure shear mode [49]. Poly vinyl alcohol (PVA) hydrogels and hydrogel-based scaffolds have been extensively investigated for cartilage tissue engineering [50,51]. In these kinds of usages, hydrogels bear the shear and unconfined com-

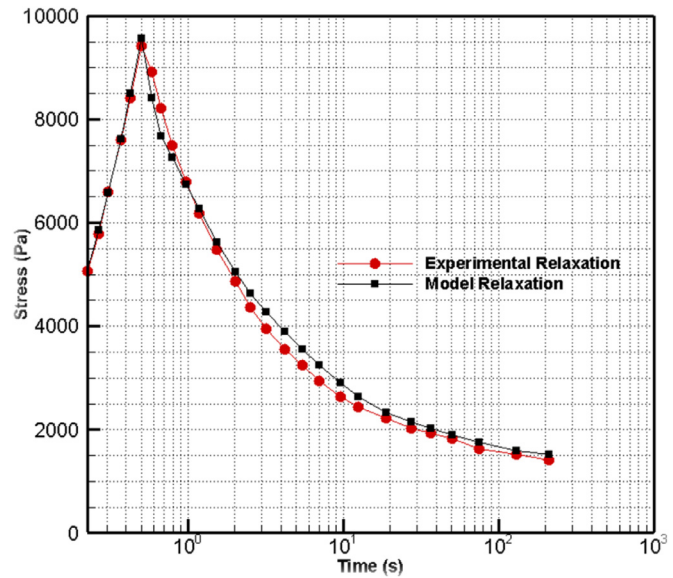


**Fig. 6.** Comparison of relaxation prediction and experimental data [8].

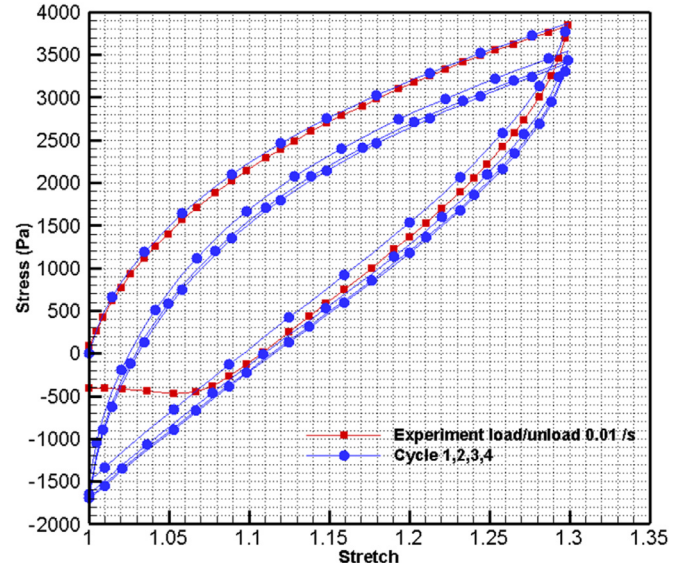


**Fig. 7.** Experimental results [8] and model prediction of four loading-unloading cycles of hydrogel.

pression states and the mechanical response could be predicted with the current model.

It is important to discover the minimum and maximum strain rates that beyond of them the stress response of material does not depend on the strain rate significantly. Fig. 5 represents the stress-stretch response of the hydrogel in different strain rates. Referring to Fig. 5 it is understood that below the strain rates of 0.003/s and above of 3/s, no significant differences in the stress-stretch curve is observed; therefore, the strain rates 0.003/s and 3/s could be considered as the strain rate range that the viscoelastic effect should be considered.

Taking into account the appropriate fitting and material stability of the model, the relaxation test was modeled and the results were compared with the experimental data (Fig. 6). To simulate the relaxation test, two loading steps were considered. In the first step, the tensile deformation kinematic at the strain rate of 0.4/s was imposed to obtain the strain level of 20%. In the second step, the deformation was kept constant and the stress was relaxed by elapsing of time. It could be observed

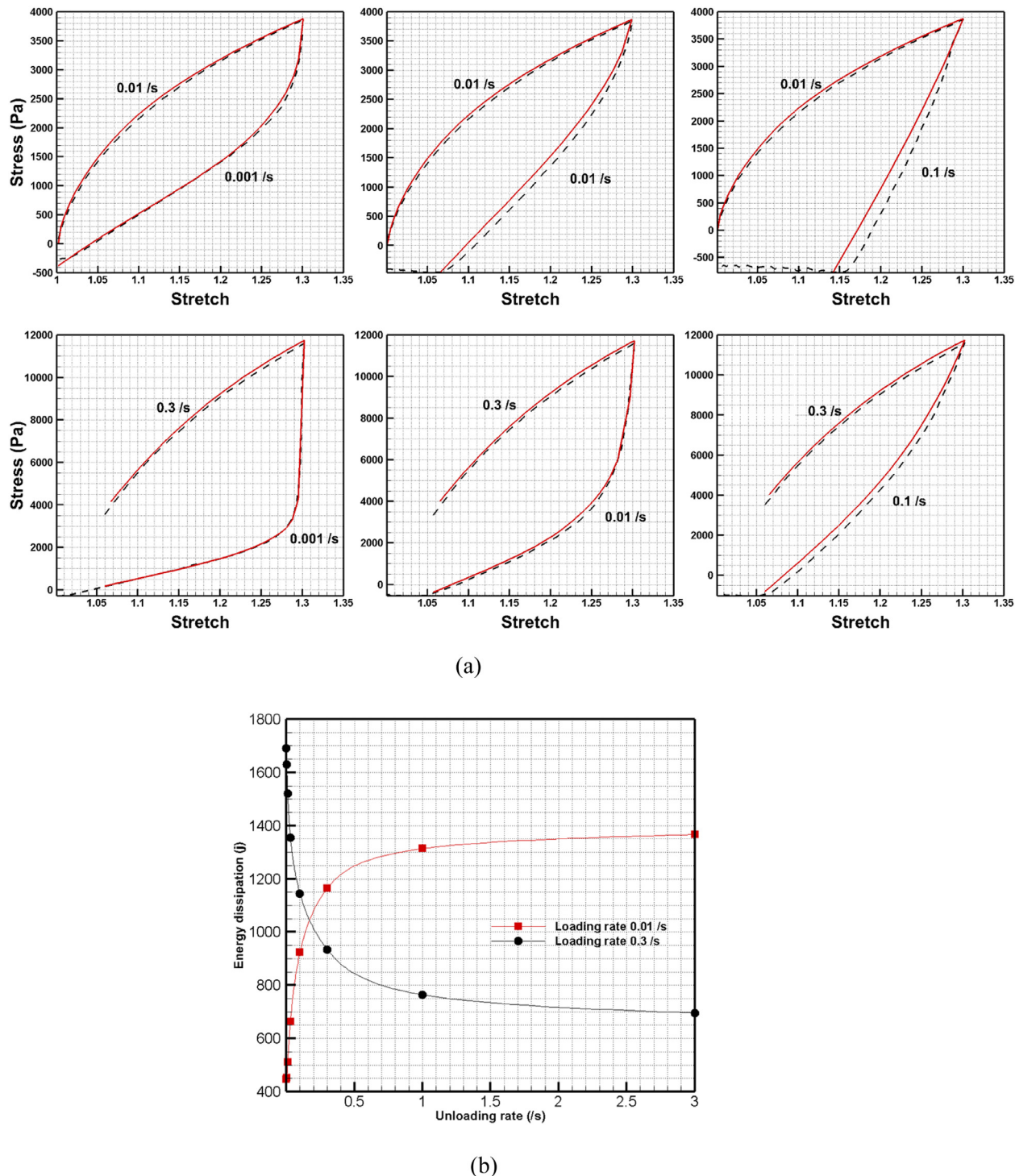


**Fig. 8.** (a) Model predictions (solid lines) and experimental data (dashed lines) [8] at different strain rates and (b) Hydrogel energy dissipation at different rates.

from Fig. 6 that after 70 s stress and the material reaches its equilibrium state.

### 5.2. Preconditioning cycles

Preconditioning occurs due to the change of the internal structure of the dual cross link hydrogel with deformation. By repeated cycling, eventually, a steady state condition is reached at which no spreading of hysteresis loop is observed unless the cycling routine changes [52]. Many researchers performed preconditioning before experimental tests

on the soft tissues [53–55]. By using the hyper-viscoelastic model, the number of cycles for preconditioning of the dual cross link self-healing hydrogel was predicted. To this goal, the sample was subjected to 30% strain at the strain rate of 0.01/s in both loading and unloading and the results were shown in Fig. 5.

As it could be seen from Fig. 7 the material behavior in the third and fourth cycles are very close to each other. Therefore, it could be concluded that at least three cycles for preconditioning of the dual self-healing hydrogel is necessary. It is worth to mention the hysteresis loops are appeared due to the viscous behavior of the material and a

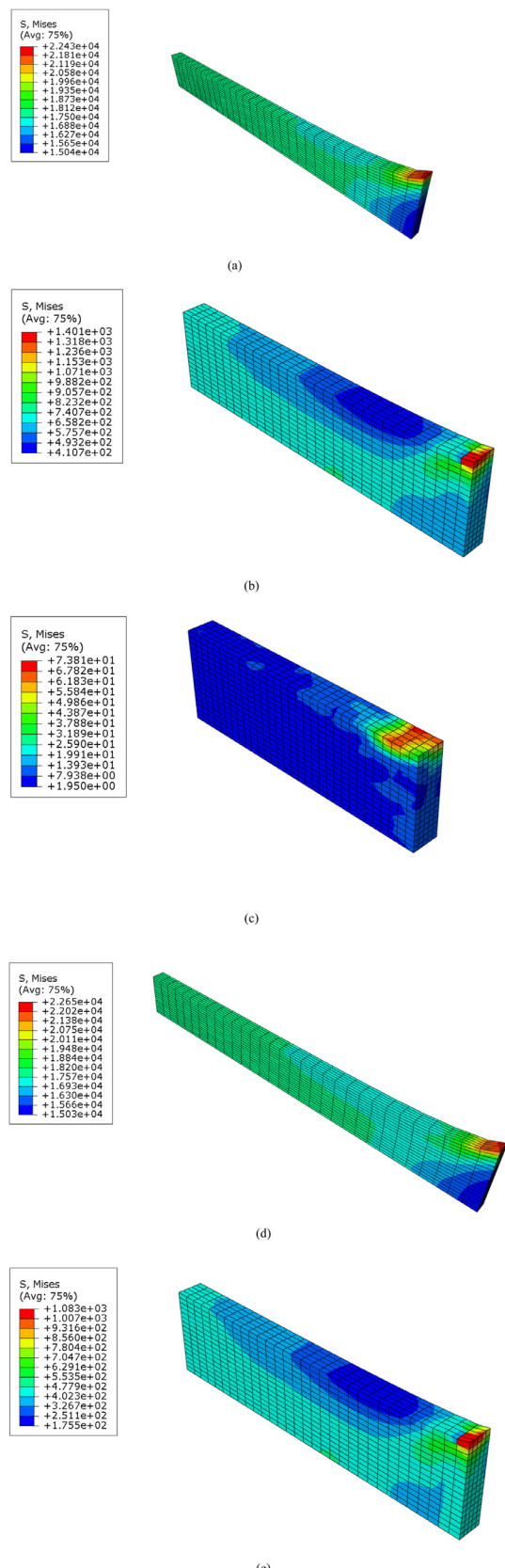


**Fig. 9.** Healing simulation: (a) first cycle loading, (b) first cycle unloading, (c) healing for 1800s, (d) and (e) same cycles as parts (a) and (b).

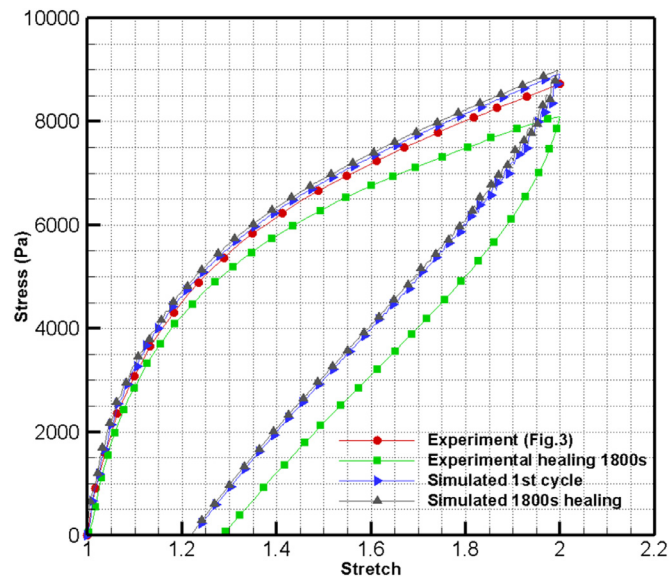


**Fig. 10.** Comparison of healing simulation and Experimental data [8].

hyperelastic model cannot capture this behavior. Also, inspection of the results of Fig. 7 reveals that in the unload regime below the stretch of 1.07 (equivalent to 7% strain) the experimental data deviates from the predictions; because the unloading should be performed at strain rate of 0.01/s, but near to the undeformed states this condition could not be controlled in experiments accurately. However, in the modeling the unloading strain rate was kept constant by imposing the boundary condition to the undeformed state.

The area between loading and unloading curves could be considered as the dissipated energy in a closed loop of deformation and sometimes this behavior is used in the anti-shock devices [56]. In Fig. 8a a good agreement between the experimental and model results at different strain rates in loading and unloading could be seen. From the data of Fig. 8a and some other similar curves that are not represented here for the sake of brevity, the dissipated energy during deformation was calculated by the energy difference between the loading and unloading branches (Fig. 8b). Results of Fig. 8b represents two different trends for the energy dissipation versus unload rate in two different loading rates. In the case of low loading rate, by increasing the unloading rate the energy dissipation is increased. However, in high loading rates, dissipated energy is decreased by increasing the unloading rate. Of course, in both low and high loading rate, a saturation in energy dissipation above the unloading strain rate of 2/s could be observed. Because in the low loading rates, there is enough time in the loading step for the healing and the dissipated energy reduces with respect to the high loading rates (see Fig. 8a at low and high loading rates).

### 5.3. Healing simulation

Healing occurs owing to the physical bond reattachment in self-healing hydrogel and thereby prediction of the healing phenomenon is important in engineering applications [8]. The time dependent part of the proposed model could take into account the healing because in a fixed deformation, stress decays as a function of time. To simulate the healing phenomenon, five steps were defined in the ABAQUS software. In the first step, the sample was stretched to the strain of 100% in the constant strain rate of 0.03/s. In the second step, the specimen was returned to the unstress state with the same strain rate to consider the unloading cycle. In the third step, the healing procedure was taken into account by the free boundary condition during 1800s to obey the same condition as Long et al. [8]. In the fourth and fifth steps, the same loading and unloading cycles were repeated. The simulation results were

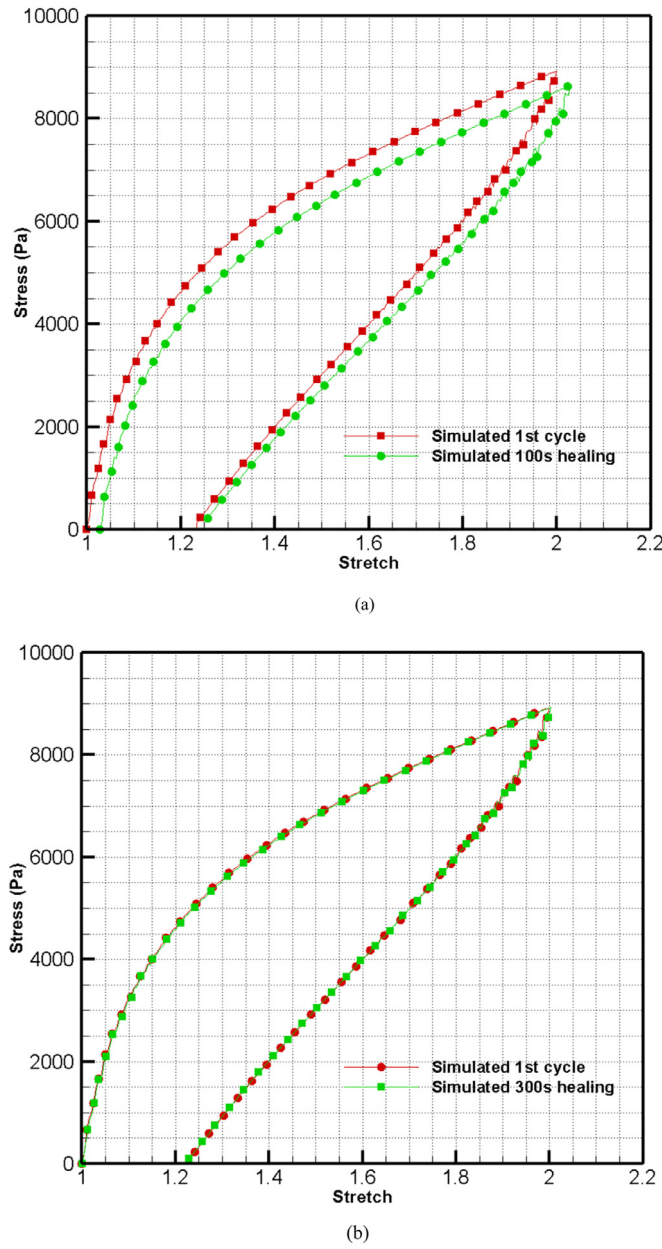


**Fig. 11.** Healing simulation for different healing time: (a) 100 s and (b) 300 s.

shown in Fig. 9. From the nodal reaction forces and displacement of the stretched side, the stress-stretch curve of the cyclic loading was prepared and the results were reported in Fig. 10.

From Fig. 10 it could be seen there is a small difference between the simulation and experimental results of healing phenomenon. However, when the loading part of the cyclic loading of Fig. 10 is compared with the monotonic loading of Fig. 3 at strain rate of 0.03/s, a good agreement could be observed. This means in the same loading rate of 0.03/s two different experimental data have been reported in Long et al. may be due to two different samples. It is worth mentioning that as we determined the model parameters from the monotonic data and thereby the accommodation in the loading part could be expected. However, as it could be conceived from Fig. 10, there is no significant difference between the first and second cycles after 1800s. Therefore, it could be ensured that in 1800s the full healing occurs. This finding is in agreement with the what was obtained by Long et al. in their experimental tests [8]. The results of Fig. 9a and d proof the healing phenomenon as the same stress distribution in the first and fourth steps could be seen.

To study the effect of healing time on the stress recovery, simulations with the healing time of 100 s and 300 s was performed and the results were illustrated in Fig. 11.

As it is indicated from Fig. 11, the specimen is not fully recovered during 100 s, but it is recovered completely during 300 s. Therefore, it is not necessary to keep the specimen in rest for 1800s. The proper estimation of the healing time should be considered, as in many applications subsequent deformations should be done after the healing. It is worth to mention in the future works it will be tried to consider the damage during the cyclic loading and as it is known the damage phenomenon impacts the healing time.

## 6. Conclusion

In this research, a hyper-viscoelastic model based on the polynomial-logarithmic strain energy function was implemented to investigate the nonlinear time-dependent behavior of the dual cross link self-healing hydrogel. The material parameters were calculated by fitting the experimental results from tension test at different strain rates. The predicted results showed good agreement with experimental data in addition to the material stability in the pure shear and balance biaxial deformation modes. It was found below the strain rates of 0.003/s the time dependency has no significant impact on the stress-stretch curves. The determined material parameters were used to predict the stress relaxation of hydrogel and it was found during the 70 s the equilibrium stress could be achieved. The results of preconditioning simulation revealed that at least three cycles are necessary to obtain the preconditioned state. In addition, it was observed the loading and unloading rate is important in energy dissipation and two distinct trends for energy dissipation in different strain rates were observed. Finally, the healing phenomenon was simulated and it was observed 300 s is needed to sample recover its initial state.

## Acknowledgements

The authors would like to thank the K. N. Toosi University of Technology, Tehran, Iran, for the financial support and research facilities used in this work.

## References

- [1] Hussain I, Sayed SM, Liu S, Oderinde O, Yao F, Fu G. Glycogen-based self-healing hydrogels with ultra-stretchable, flexible, and enhanced mechanical properties via sacrificial bond interactions. *Int J Biol Macromol* 2018.
- [2] Vedaghavami A, Minooei F, Mohammadi MH, Khetani S, Kolahchi AR, Mashayekhan S, Sanati-Nezhad A. Manufacturing of hydrogel biomaterials with controlled mechanical properties for tissue engineering applications. *Acta Biomater* 2017;62:42–63.
- [3] Li M, Jiang Z, An N, Zhou J. Harnessing programmed holes in hydrogel bilayers to design soft self-folding machines. *Int J Mech Sci* 2018;140:271–8.
- [4] Sahraro M, Barikani M, Daemi H. Mechanical reinforcement of Gellan gum poly-electrolyte hydrogels by cationic polyurethane soft nanoparticles. *Carbohydr Polym* 2018.
- [5] Xiang H, Xia M, Cunningham A, Chen W, Sun B, Zhu M. Mechanical properties of biocompatible clay/P (MEO2MA-co-OEGMA) nanocomposite hydrogels. *J Mech Behav Biomed Mater* 2017;72:74–81.
- [6] Mayumi K, Marcellan A, Ducouret G, Creton C, Narita T. Stress–strain relationship of highly stretchable dual cross-link gels: separability of strain and time effect. *ACS Macro Lett* 2013;2:1065–8.
- [7] Qin Z, Niu R, Tang C, Xia J, Ji F, Dong D, Zhang H, Zhang S, Li J, Yao F. A dual-crosslinked strategy to construct physical hydrogels with high strength, toughness, good mechanical recoverability, and shape-memory ability. *Macromol Mater Eng* 2018;303:1700396.
- [8] Long R, Mayumi K, Creton C, Narita T, Hui C-Y. Time dependent behavior of a dual cross-link self-healing gel: theory and experiments. *Macromolecules* 2014;47:7243–50.
- [9] Madireddy S, Sista B, Vemaganti K. A Bayesian approach to selecting hyperelastic constitutive models of soft tissue. *Comput Meth Appl Mech Eng* 2015;291:102–22.
- [10] Darijani H, Naghdabadi R. Hyperelastic materials behavior modeling using consistent strain energy density functions. *Acta Mech* 2010;213:235–54.
- [11] Hosseinzadeh M, Ghoreishi M, Narooei K. Investigation of hyperelastic models for nonlinear elastic behavior of demineralized and deproteinized bovine cortical femur bone. *J Mech Behav Biomed Mater* 2016;59:393–403.

- [12] Elyasi N, Taheri KK, Narooei K, Taheri AK. A study of hyperelastic models for predicting the mechanical behavior of extensor apparatus. *Biochem Model Mechanobiol* 2017;16:1077–93.
- [13] Sasson A, Patchornik S, Eliasy R, Robinson D, Haj-Ali R. Hyperelastic mechanical behavior of chitosan hydrogels for nucleus pulposus replacement—Experimental testing and constitutive modeling. *J Mech Behav Biomed Mater* 2012;8:143–53.
- [14] Hamzehei R, Kadkhodapour J, Anaraki AP, Rezaei S, Dariushi S, Rezadoust AM. Octagonal auxetic metamaterials with hyperelastic properties for large compressive deformation. *Int J Mech Sci* 2018;145:96–105.
- [15] Zhao W, Shi Z, Chen X, Yang G, Lenardi C, Liu C. Microstructural and mechanical characteristics of PHEMA-based nanofibre-reinforced hydrogel under compression. *Compos Part B Eng* 2015;76:292–9.
- [16] Kancz Y, Milner P, Dini D, Amis AA. Tribological properties of PVA/PVP blend hydrogels against articular cartilage. *J Mech Behav Biomed Mater* 2018;78:36–45.
- [17] Suriano R, Griffini G, Chiari M, Levi M, Turri S. Rheological and mechanical behavior of polyacrylamide hydrogels chemically crosslinked with allyl agarose for two-dimensional gel electrophoresis. *J Mech Behav Biomed Mater* 2014;30:339–46.
- [18] Liu K, Ovaert TC. Poro-viscoelastic constitutive modeling of unconfined creep of hydrogels using finite element analysis with integrated optimization method. *J Mech Behav Biomed Mater* 2011;4:440–50.
- [19] Gao X, Kuśmierczyk P, Shi Z, Liu C, Yang G, Sevostianov I, Silberschmidt VV. Through-thickness stress relaxation in bacterial cellulose hydrogel. *J Mech Behav Biomed Mater* 2016;59:90–8.
- [20] Caccavo D, Lamberti G. PoroViscoElastic model to describe hydrogels' behavior. *Mater Sci Eng C* 2017;76:102–13.
- [21] Caccavo D, Cascone S, Poto S, Lamberti G, Barba AA. Mechanics and transport phenomena in agarose-based hydrogels studied by compression-relaxation tests. *Carbohydr Polym* 2017;167:136–44.
- [22] Xin H, Brown HR, Naficy S, Spinks GM. Time-dependent mechanical properties of tough ionic-covalent hybrid hydrogels. *Polymer* 2015;65:253–61.
- [23] Forte A, D'Amico F, Charalambides M, Dini D, Williams J. Modelling and experimental characterisation of the rate dependent fracture properties of gelatine gels. *Food Hydrocolloids* 2015;46:180–90.
- [24] Tomita Y, Nakata S, Honma T, Yashiro K. Deformation behavior of silica-filled rubber with coupling agents under monotonic and cyclic straining. *Int J Mech Sci* 2014;86:7–17.
- [25] Tirella A, Mattei G, Ahluwalia A. Strain rate viscoelastic analysis of soft and highly hydrated biomaterials. *J Biomed Mater Res Part A* 2014;102:3352–60.
- [26] Ravikumar N, Noble C, Cramphorn E, Taylor ZA. A constitutive model for ballistic gelatin at surgical strain rates. *J Mech Behav Biomed Mater* 2015;47:87–94.
- [27] Narooei K, Arman M. Generalization of exponential based hyperelastic to hyper-viscoelastic model for investigation of mechanical behavior of rate dependent materials. *J Mech Behav Biomed Mater* 2017.
- [28] Goh S, Charalambides M, Williams J. Determination of the constitutive constants of non-linear viscoelastic materials. *Mech Time-Depend Mater* 2004;8:255–68.
- [29] Karimi A, Navidbakhsh M, Razaghi R. An experimental-finite element analysis on the kinetic energy absorption capacity of polyvinyl alcohol sponge. *Mater Sci Eng C* 2014;39:253–8.
- [30] Wang Q, Gao Z. A constitutive model of nanocomposite hydrogels with nanoparticle crosslinkers. *J Mech Phys Solids* 2016;94:127–47.
- [31] Dorfmann A, Ogden RW. A constitutive model for the Mullins effect with permanent set in particle-reinforced rubber. *Int J Solids Struct* 2004;41:1855–78.
- [32] Lu T, Wang J, Yang R, Wang T. A constitutive model for soft materials incorporating viscoelasticity and Mullins effect. *J Appl Mech* 2017;84:021010.
- [33] Gefen A, Margulies SS. Are *in vivo* and *in situ* brain tissues mechanically similar? *J Biomech* 2004;37:1339–52.
- [34] Benítez JM, Montáns FJ. The mechanical behavior of skin: structures and models for the finite element analysis. *Comp Struc* 2017;190:75–107.
- [35] Kousa P, Järvinen TL, Vihamäki M, Kannus P, Järvinen M. The fixation strength of six hamstring tendon graft fixation devices in anterior cruciate ligament reconstruction: part I: femoral site. *Am J Sports Med* 2003;31:174–81.
- [36] Johnson B, Beebe D, Crone W. Effects of swelling on the mechanical properties of a pH-sensitive hydrogel for use in microfluidic devices. *Mater Sci Eng C* 2004;24:575–81.
- [37] Marra S, Ramesh K, Douglas A. Mechanical characterization of active poly (vinyl alcohol)-poly (acrylic acid) gel. *Mater Sci Eng C* 2001;14:25–34.
- [38] Millon L, Mohammadi H, Wan W. Anisotropic polyvinyl alcohol hydrogel for cardiovascular applications. *J Biomed Mater Res Part B Appl Biomater* 2006;79:305–11.
- [39] Narooei K, Arman M. Modification of exponential based hyperelastic strain energy to consider free stress initial configuration and Constitutive modeling. *J Mech Behav Biomed Mater* 2018;49:189–96.
- [40] Khajehsaeid H, Arghavani J, Naghdabadi R, Sohrabpour S. A visco-hyperelastic constitutive model for rubber-like materials: a rate-dependent relaxation time scheme. *Int J Eng Sci* 2014;79:44–58.
- [41] Mooney M. A theory of large elastic deformation. *J Appl Phys* 1940;11:582–92.
- [42] Ogden RW. Non-linear elastic deformations. Courier Corporation; 1997.
- [43] Belytschko T, Liu WK, Moran B, Elkhodary K. Nonlinear finite elements for continua and structures. John wiley & sons; 2013.
- [44] Yang L, Shim V. A visco-hyperelastic constitutive description of elastomeric foam. *Int J Impact Eng* 2004;30:1099–110.
- [45] Motallebzadeh H, Charlebois M, Funnell WRJ. A non-linear viscoelastic model for the tympanic membrane. *J Acoust Soc Am* 2013;134:4427–34.
- [46] Ghereishy MHR. Determination of the parameters of the Prony series in hyper-viscoelastic material models using the finite element method. *Mater Design* 2012;35:791–7.
- [47] Fahimi S, Baghani M, Zakerzadeh M-R, Eskandari A. Developing a visco-hyperelastic material model for 3D finite deformation of elastomers. *Finite Elem Anal Des* 2018;140:1–10.
- [48] Ogden R, Saccomandi G, Sgura I. Fitting hyperelastic models to experimental data. *Comput Mech* 2004;34:484–502.
- [49] Horgan CO, Smady MG. The importance of the second strain invariant in the constitutive modeling of elastomers and soft biomaterials. *Mech Mater* 2012;51:43–52.
- [50] Stammen JA, Williams S, Ku DN, Guldberg RE. Mechanical properties of a novel PVA hydrogel in shear and unconfined compression. *Biomaterials* 2001;22:799–806.
- [51] Wan LQ, Jiang J, Miller DE, Guo XE, Mow VC, Lu HH. Matrix deposition modulates the viscoelastic shear properties of hydrogel-based cartilage grafts. *Tissue Eng Part A* 2011;17:1111–22.
- [52] Fung Y-C. Biomechanics: mechanical properties of living tissues. Springer Science & Business Media; 2013.
- [53] Pazos V, Mongrain R, Tardif J. Polyvinyl alcohol cryogel: optimizing the parameters of cryogenic treatment using hyperelastic models. *J Mech Behav Biomed Mater* 2009;2:542–9.
- [54] Millon L, Wan W. The polyvinyl alcohol-bacterial cellulose system as a new nanocomposite for biomedical applications. *J Biomed Mater Res Part B Appl Biomater* 2006;79:245–53.
- [55] Samani A, Zubovits J, Plewes D. Elastic moduli of normal and pathological human breast tissues: an inversion-technique-based investigation of 169 samples. *Phys Med Biol* 2007;52:1565.
- [56] Shen F, Yuan S, Guo Y, Zhao B, Bai J, Qwamizadeh M, Chua CK, Wei J, Zhou K. Energy absorption of thermoplastic polyurethane lattice structures via 3D printing: modeling and prediction. *Int J Appl Mech* 2016;8:1640006.